Electronic Supplementary Information

Naphthyridine-based emitters simultaneously exhibiting thermally activated delayed fluorescence and aggregation-induced emission for highly efficient non-doped fluorescent OLEDs

Xue Zhou [a,b], Hannan Yang [c], Zhanxiang Chen [a], Shaolong Gong [a]*, Zheng-Hong Lu [c]* and Chuluo Yang [a,b]*

[a] Department of Chemistry, Hubei Key Laboratory on Organic and Polymeric Optoelectronic Materials, Wuhan University, Wuhan 430072, People's Republic of China

[b] Shenzhen Key Laboratory of Polymer Science and Technology, College of Materials Science and Engineering, Shenzhen University, Shenzhen 518060, People's Republic of China

[c] Department of Physics, Yunnan Key Laboratory for Micro/Nano Materials and Technology, Yunnan University, Kunming 650091, People's Republic of China

General information

All chemical reagents were purchased from commercial chemical companies and used without further purification unless it was necessary. The reactions and manipulations susceptive to moisture and oxygen were carried out under the protection of argon. The 400 MHz ^{1}H and 100 MHz ^{13}C nuclear magnetic resonance (NMR) spectra were recorded on a Bruker AV-500 (400 MHz) in deuterated chloroform with tetramethyl-silane (TMS) as an internal reference. High-resolution mass spectrometry (HRMS) spectra was measured by LCQ-Orbitrap Elite (Thermo-Fisher Scientific, Waltham, MA, USA) mass spectrometer. Thermogravimetric analysis (TGA) was recorded on a NEZSCH STA 449C instrument under nitrogen atmosphere at a heating rate of 10 ^{o}C/min from 25 ^{o}C to 650 ^{o}C. The temperature of degradation (T_d) was correlated to a 5% weight loss. Cyclic voltammetry (CV) data were measured on a CHI630E electrochemical workstation equipped with a glassy carbon working electrode, a saturated calomel electrode as the reference electrode, and a platinum wire counter electrode. The measurements were carried out with anhydrous acetonitrile tetrabutylammoniumhexafluorophosphate (0.1 M) as the supporting electrolyte at a scan rate of 100 mV s^{-1}. Potentials were referenced to the ferrocene/ferrocenium couple by using ferrocene as the standard. The fermi level of ferrocene was set at -4.80 eV with respect to zero vacuum level. UV-vis absorption spectra were obtained with a Shimadzu UV-3600 UV-vis-NIR spectrometer. Photoluminescence (PL) spectra were recorded on a Hitachi F-4600 fluorescence spectrophotometer. The PL lifetimes were measured by a single photon counting spectrometer from Edinburgh Instruments (FLS920) with a Picosecond Pulsed UV-LASTER

(LASTER377) as the excitation source. The samples were placed in a vacuum cryostat chamber with the temperature control. The solid state absolute photoluminescence quantum yields (PLQYs) were measured on a Quantaurus-QY measurement system (C9920-02, Hamamatsu Photonics) equipped with a calibrated integrating sphere in the host of CBP and all the samples were excited at 330 nm.

Device fabrication and characterization

The hole-transporting material of 1,1-bis[(di-4-tolylamino)phenyl]cyclohexane (TAPC), assistant hole-transporting material of 4,4′,4″-tri(*N*-carbazolyl)triphenylamine (TCTA), host material of 4,4′-di(9*H*-carbazol-9-yl)-1,1′-biphenyl (CBP), electron-transporting material of 1,3,5-tri(*m*-pyrid-3-yl-phenyl)benzene (Tm3PyPB) were commercially bought from Luminescence Technology Corporation and used as received. The electron-injection material of LiF was purchased from Sigma-Aldrich and used as received. All of the devices were fabricated in a tri-chamber high-vacuum system without breaking vacuum, under a base pressure of 10^{-7} Torr. Commercial patterned indium tin-oxide (ITO)-coated glass with a sheet resistance of 15 Ω per square was used as the basis substrate. Before device fabrication, the substrate was pre-cleaned sequentially using Alconox, acetone, and methanol for 5 min in each step, blow-dried with a N^2 gun, and surface activated using a UV-ozone chamber. All doping concentrations used in this work are weight percentage. The active area for all devices was 2 mm^2. Luminance-voltage measurements were performed with a Minolta LS-110 Luminance Meter. Current-voltage characteristics were measured using an HP4140B picoammeter. The electroluminescence spectra were recorded with an Ocean Optics USB-4000 spectrometer.

Synthesis of materials

All reagents were used as received from commercial sources and used as received unless otherwise stated.

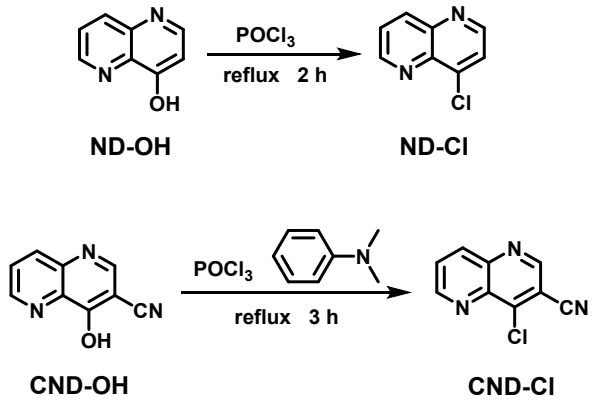

Scheme S1. Synthesis route of ND-Cl and CND-Cl

Synthesis of 4-Hydroxy-1,5-naphthyridine (ND-OH) and 4-Hydroxy-1,5-naphthyridine-3-carbonitrile (CND-

OH) was carried out by referencing the reported literature.

Synthesis of 4-Chloro-1,5-nathphyridine (ND-Cl): 1.44 g (10 mmol) ND-OH and 10 mL $POCl_3$ were added into a 50 mL round-bottom flask. The mixture was refluxed 2 h under the protection of argon. The reaction liquid was added dropwise into ice water under vigorous stirring conditions and then neutralized by aqueous sodium hydroxide. The mixture was extracted with dichloromethane (70 mL×4), and dried over anhydrous Na_2SO_4. After removal of the solvents, the crude product was purified by column chromatography on silica gel with dichloromethane (DCM)/ethyl acetate (4:1 v/v) containing little triethylamine as the eluent to give a white solid (0.89 g, 5.4 mmol, yield 54%). ^{1}H NMR (400 MHz, $CDCl_3$ + TMS, 25 ^{o}C) δ [ppm]: 9.11 (dd, J = 4.1, 1.6 Hz, 1H), 8.88 (d, J = 4.7 Hz, 1H), 8.47 (dd, J = 8.5, 1.6 Hz, 1H), 7.79 (d, J = 4.7 Hz, 1H), 7.75 (dd, J = 8.5, 4.2 Hz, 1H). ^{13}C NMR (100 MHz, $CDCl_3$, 25 ^{o}C) δ [ppm]: 151.67, 150.75, 144.97, 144.16, 140.93, 138.07, 125.39, 124.57.

Synthesis of 4-Chloro-1,5-naphthyridine-3-carbonitrile (CND-Cl): 1.71 g (10 mmol) CND-OH, 1.3 mL *N,N*-dimethylaniline and 10 mL $POCl_3$ were added into a 50 mL round-bottom flask. The mixture was refluxed 3 h under the protection of argon. The reaction liquid was added dropwise into ice water under vigorous stirring conditions and then neutralized by aqueous sodium hydroxide. The mixture was extracted with dichloromethane (70 mL×6), and dried over anhydrous Na_2SO_4. After removal of the solvents, the crude product was purified by column chromatography on silica gel with DCM/ethyl acetate (5:1 v/v) containing little triethylamine as the eluent to give a white solid (0.63 g, 3.3 mmol, yield 33%). ^{1}H NMR (400 MHz, $CDCl_3$ + TMS, 25 ^{o}C) δ [ppm]: 9.18 (dd, J = 4.1, 1.6 Hz, 1H), 9.02 (s, 1H), 8.49 (dd, J = 8.6, 1.6 Hz, 1H), 7.85 (dd, J = 8.6, 4.1 Hz, 1H). ^{13}C NMR (100 MHz, $CDCl_3$, 25 ^{o}C) δ [ppm]: 153.39, 150.60, 149.19, 145.93, 139.42, 138.25, 127.58, 114.10, 110.83.

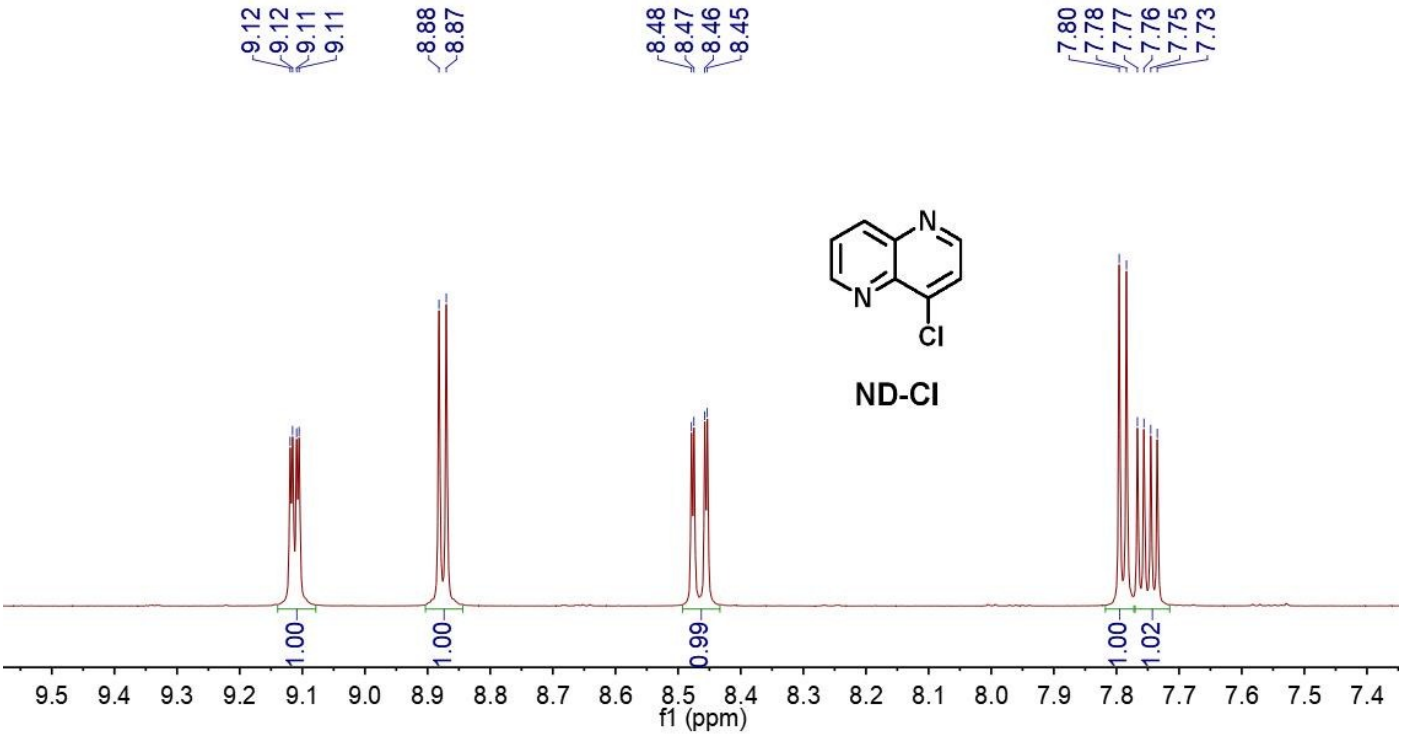

Fig. S1. ^{1}H NMR spectrum of ND-Cl (400 MHz, $CDCl_3$ + TMS, 25 ^{o}C)

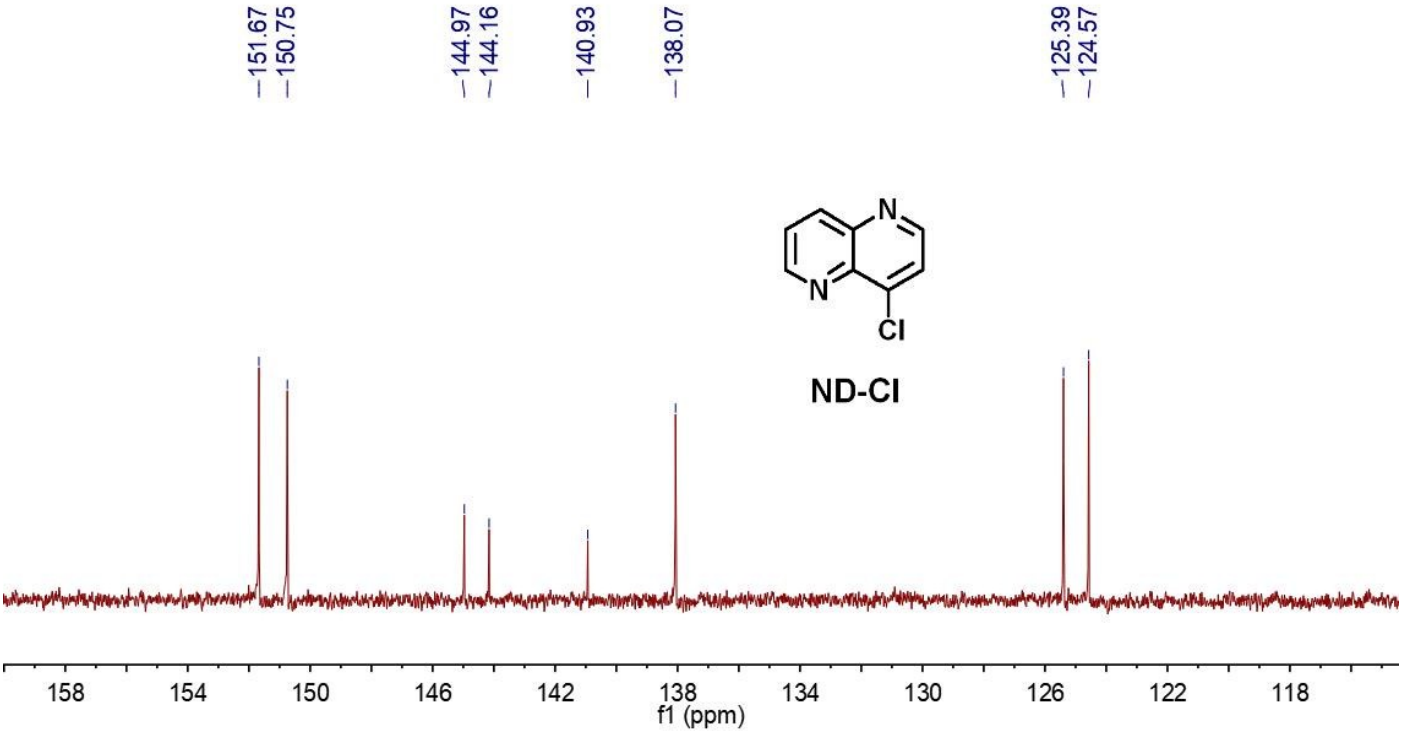

Fig. S2. ^{13}C NMR spectrum of ND-Cl (100 MHz, $CDCl_3$, 25 ^{o}C)

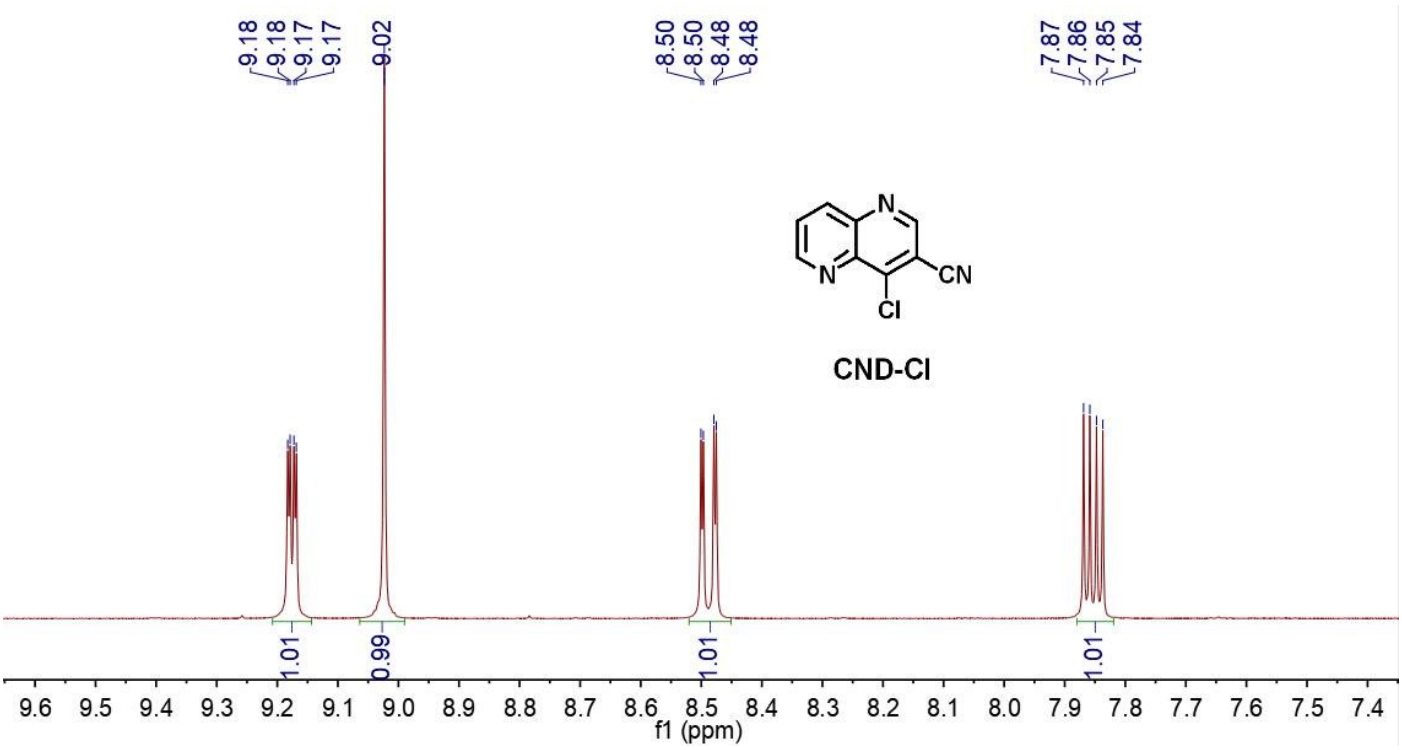

Fig. S3. ^{1}H NMR spectrum of CND-Cl (400 MHz, $CDCl_3$ + TMS, 25 ^{o}C)

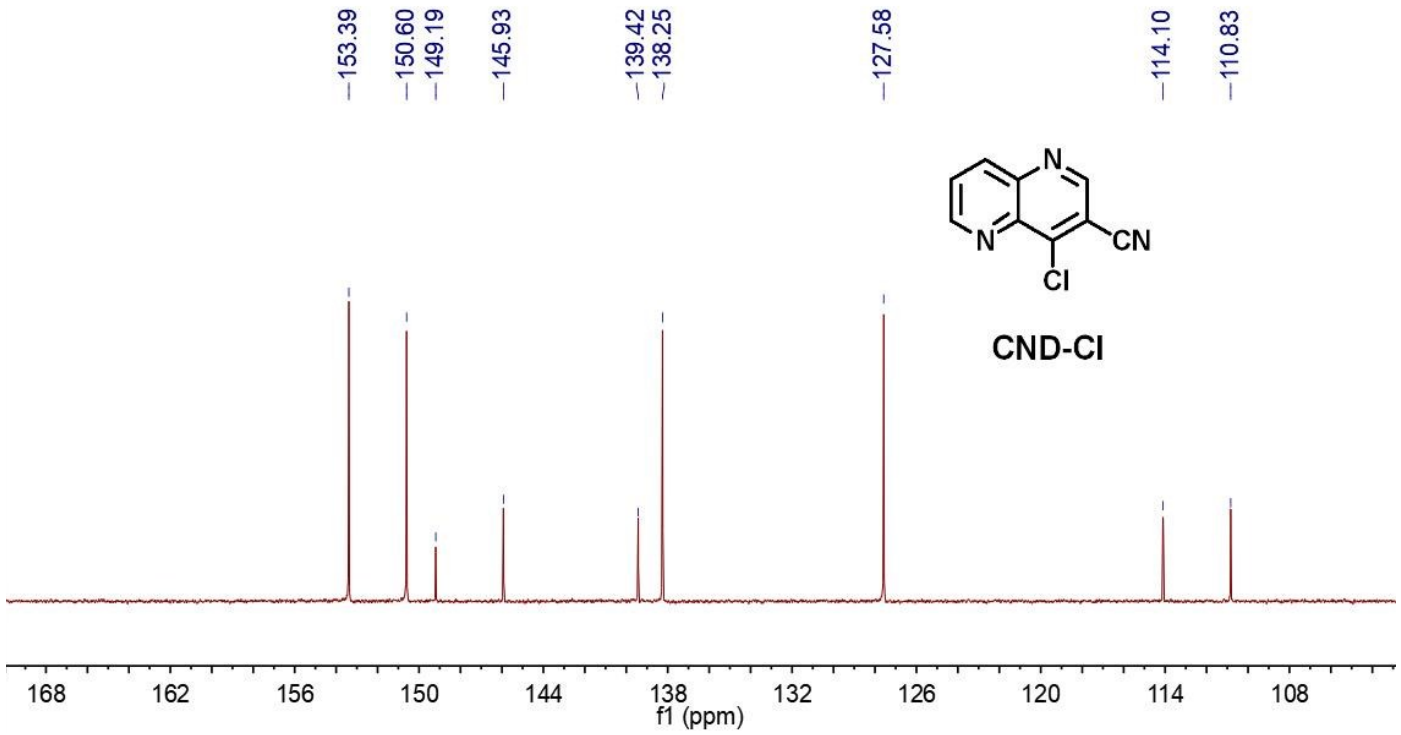

Fig. S4. ^{13}C NMR spectrum of CND-Cl (100 MHz, $CDCl_3$, 25 ^{o}C)

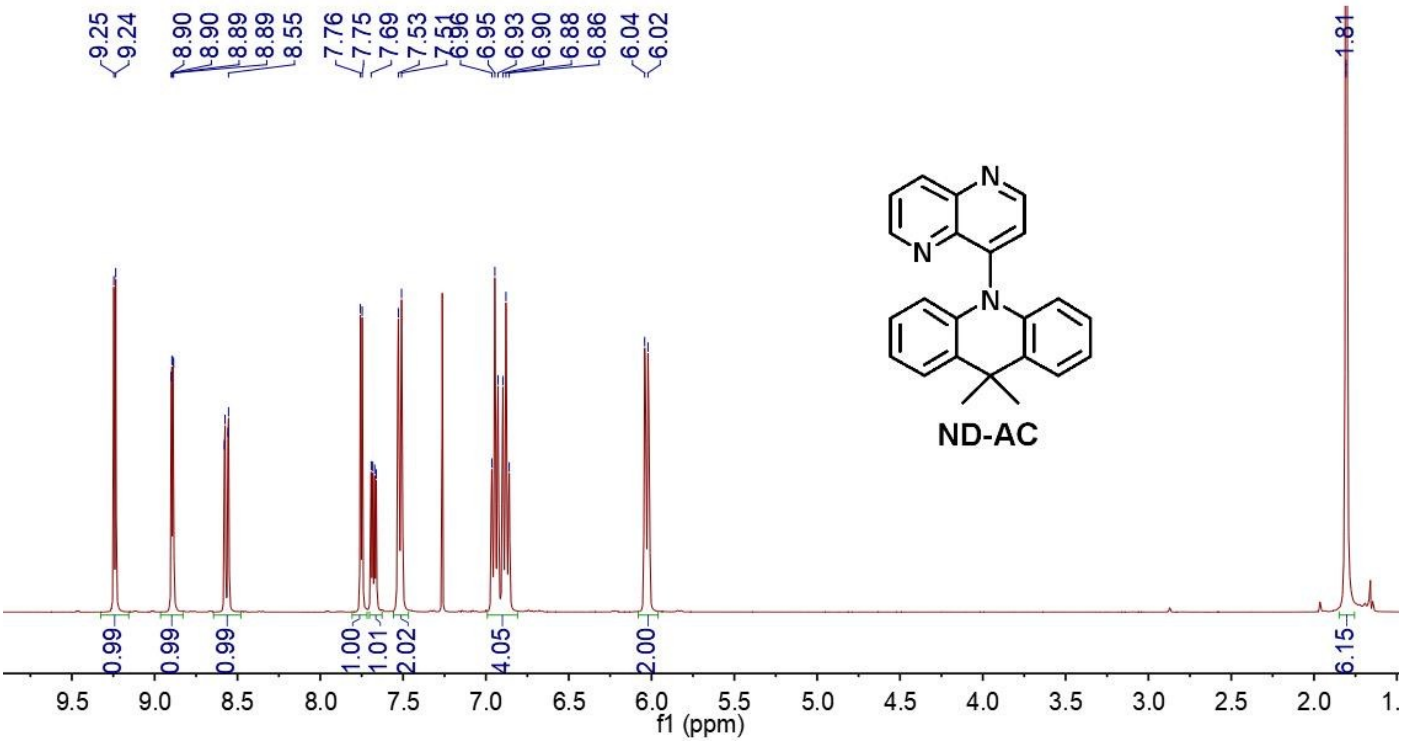

Fig. S5. ^{1}H NMR spectra of ND-AC (400 MHz, $CDCl_3$ + TMS, 25 ^{o}C)

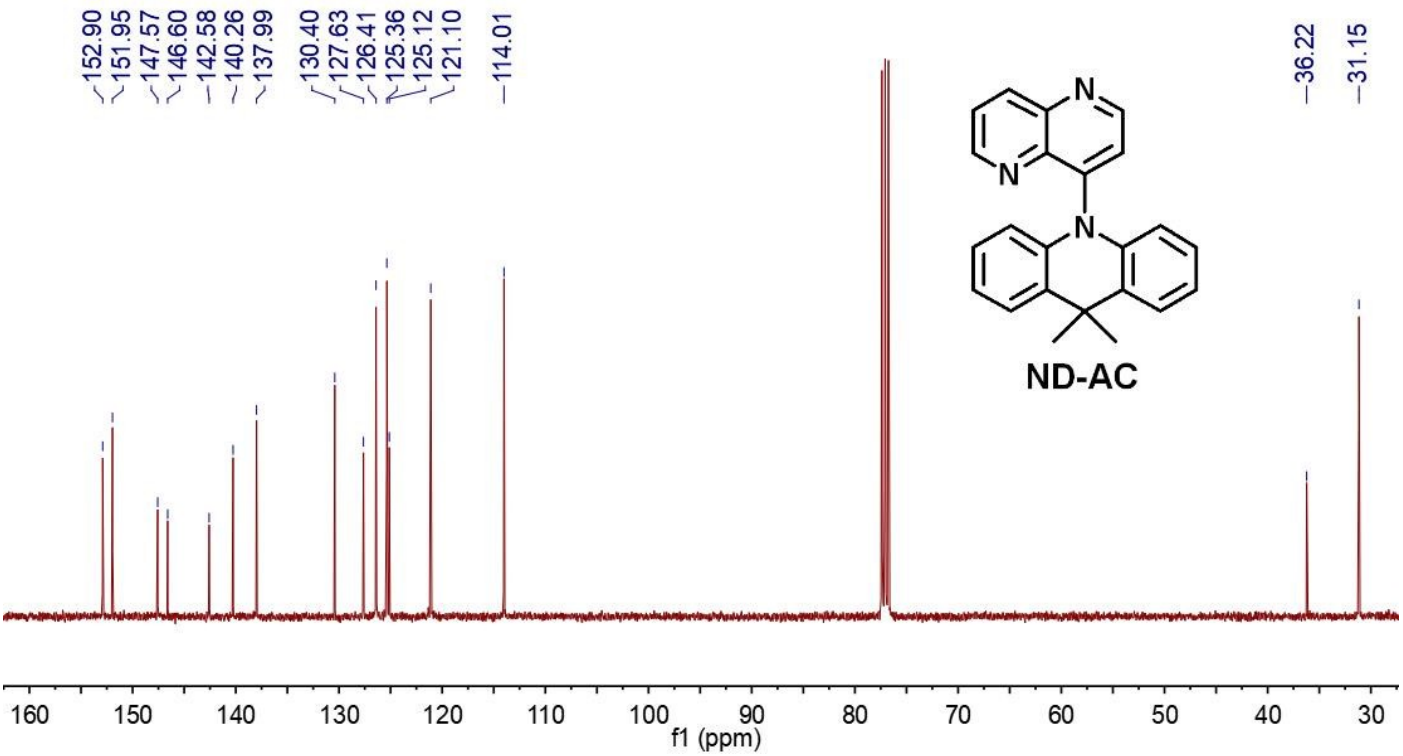

Fig. S6. ^{13}C NMR spectrum of ND-AC (100 MHz, $CDCl_3$, 25 ^{o}C)

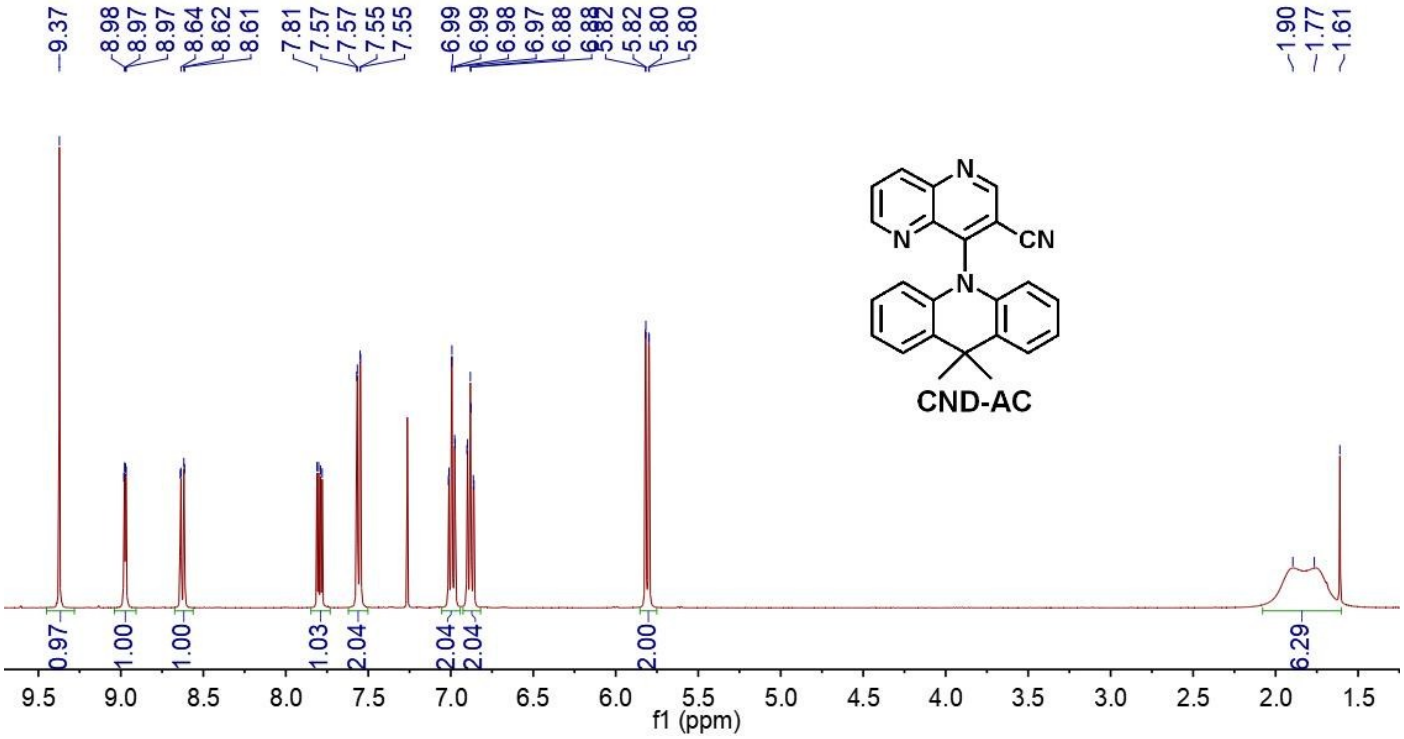

Fig. S7. ^{1}H NMR spectrum of CND-AC (400 MHz, $CDCl_3$ + TMS, 25 ^{o}C)

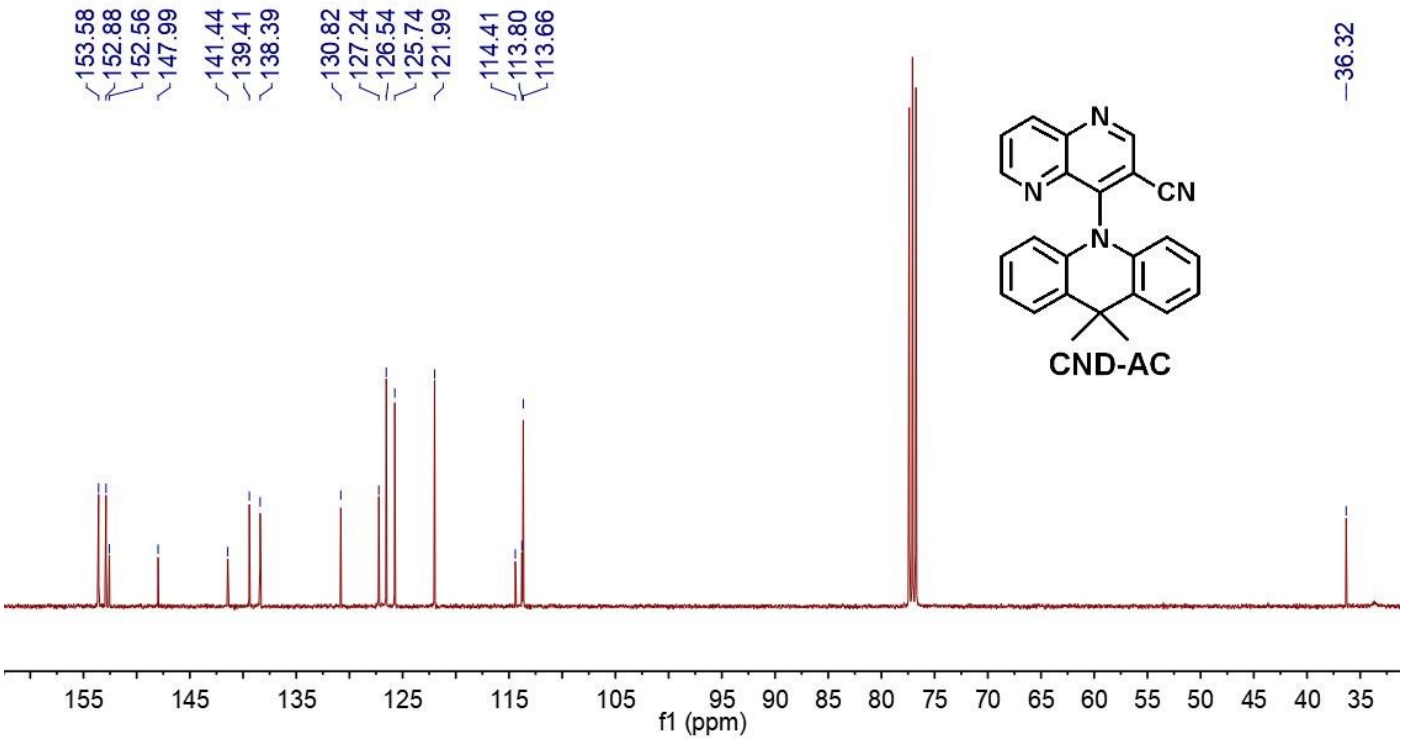

Fig. S8. ^{13}C NMR spectrum of CND-AC (100 MHz, $CDCl_3$, 25 ^{o}C)

Snow-1. HRMS (ESI) m/z calcd for $C_{23}H_{20}N_3^+$ $(M+H)^+$ 338.16517, found 338.16495.

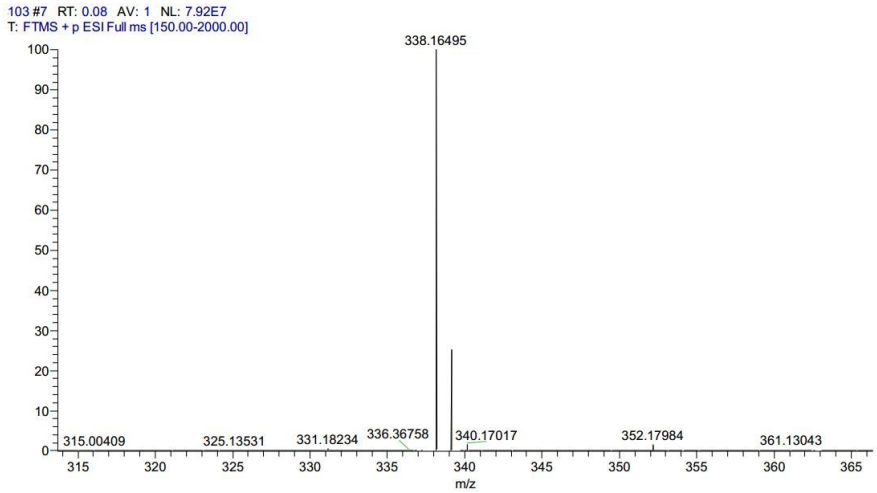

Fig. S9. High-resolution mass data of ND-AC.

Snow-2. HRMS (ESI) m/z calcd for $C_{24}H_{19}N_4^+$ $(M+H)^+$ 363.16042, found 363.16013.

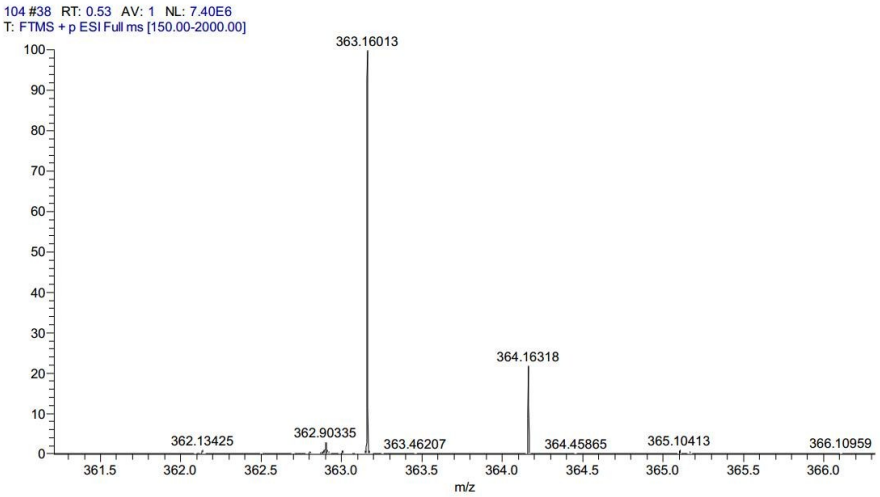

Fig. S10. High-resolution mass data of CND-AC

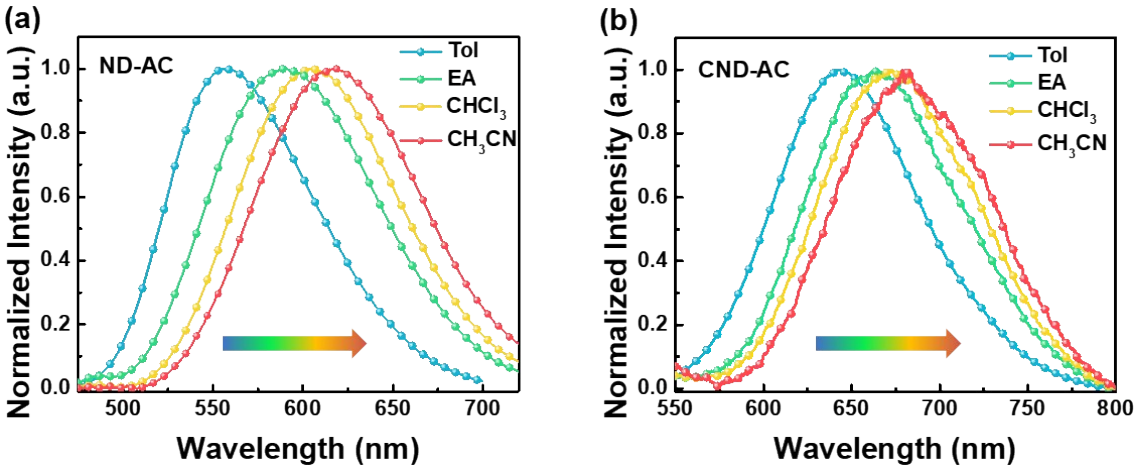

Fig. S11. Normalized PL spectra of (a) ND-AC and (b) CND-AC in toluene, ethyl acetate, $CHCl_3$ and CH_3CN.

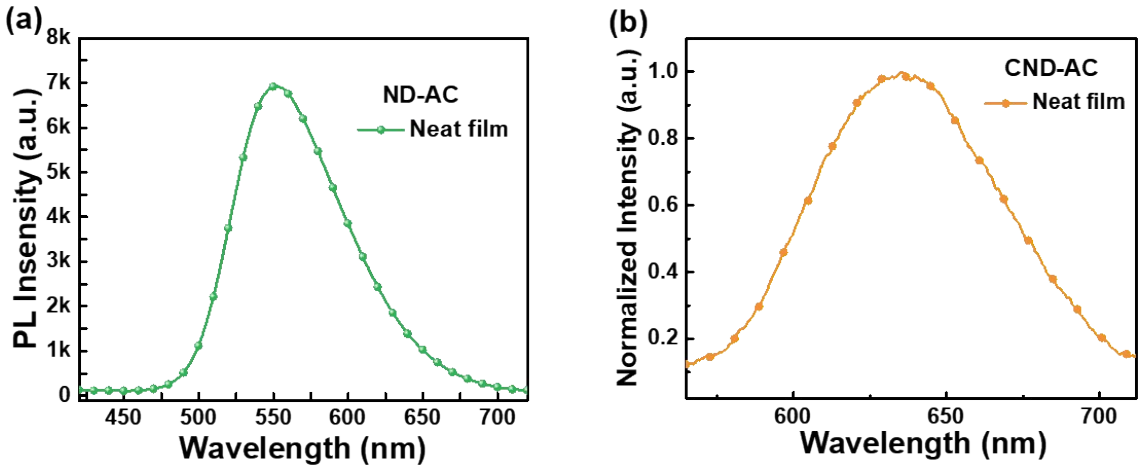

Fig. S12. The fluorescence spectra of (a) ND-AC and (b) CND-AC in neat films.

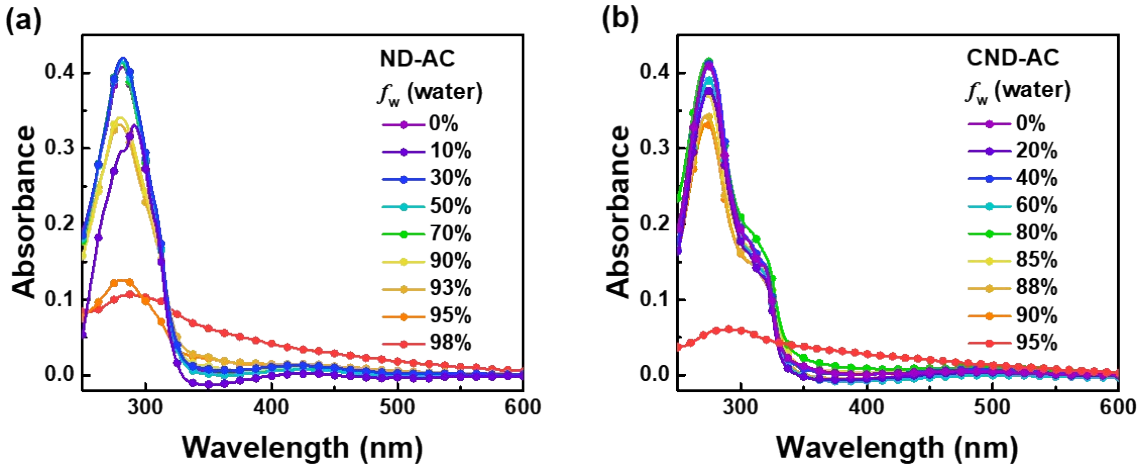

Fig. S13. The absorption spectra of (a) ND-AC and (b) CND-AC in THF/water solutions with different water fractions.

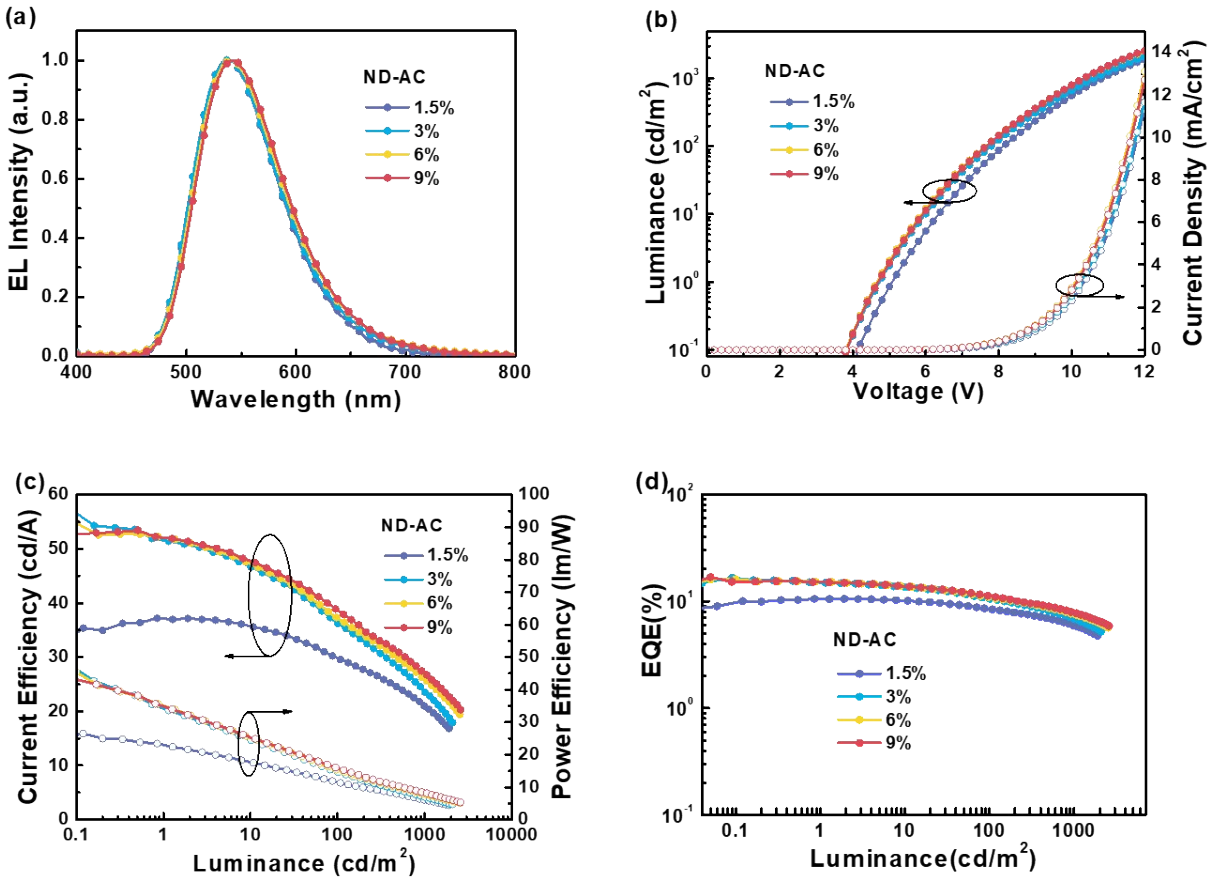

Fig. S14. The EL performance of doped devices based on ND-AC.

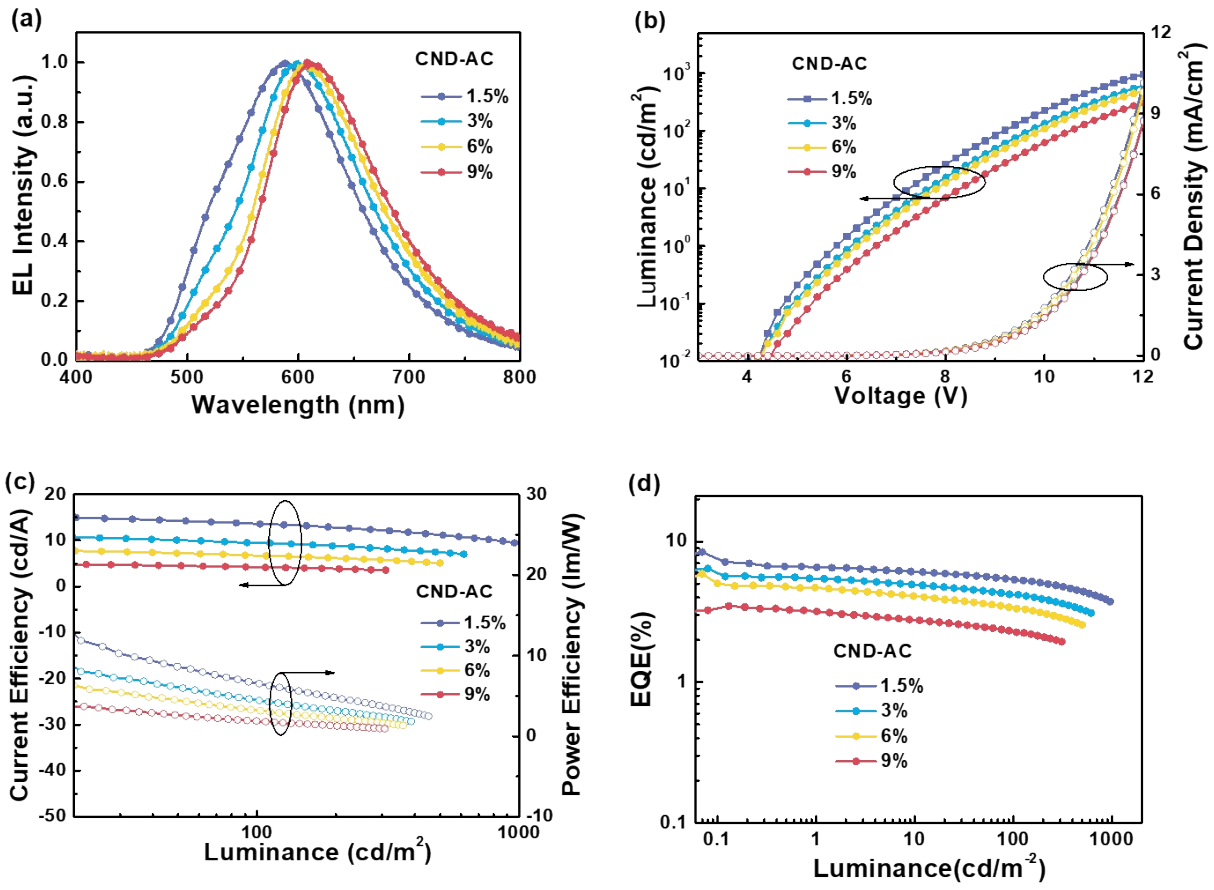

Fig. S15. The EL performance of doped devices based on CND-AC.

Table S1 The lifetime and delayed ratio of the two compounds.

Compounds	Toluene			Doped film			Neat film		
	τ_p [ns]	τ_d [μs]	delay ratio	τ_p [ns]	τ_d [μs]	delay ratio	τ_p [ns]	τ_d [μs]	delay ratio
ND-AC	22.6	0.72	68%	29.9	4.60	89%	40.4	2.98	90%
CND-AC	9.2	0.50	60%	14.5	1.02	67%	26.8	0.77	64%

$$k_p = 1/\tau_p \qquad \textbf{Eq. S1}$$

$$k_d = 1/\tau_d \qquad \textbf{Eq. S2}$$

$$k_r^S = \Phi_p k_p + \Phi_d k_d \qquad \textbf{Eq. S3}$$

$$k_{nr}^S = \frac{1-\Phi_{PL}}{\Phi_{PL}} k_r^S \qquad \textbf{Eq. S4}$$

$$k_{ISC} = \frac{\Phi_d}{\Phi_d + \Phi_p} k_p \qquad \textbf{Eq. S5}$$

$$k_{RISC} = \frac{\Phi_d}{\Phi_p} \frac{k_p k_d}{k_{ISC}} \qquad \textbf{Eq. S6}$$

Table S2 Comparison of the non-doped device performances of ND-AC and representative OLEDs with similar emissions in literatures.

Compounds	Property	CE_{max} [cd A^{-1}]	PE_{max} [lm W^{-1}]	EQE_{max} [%]	Peak [nm]	Ref.
(MesB)2DMTPS	AIE	7.4	3.2	2.25	540	Adv. Funct. Mater. 2014, 24, 3621[S1]
(MesB)2HPS	AIE	8.4	4.1	2.62	548	
(MesB)2MPPS	AIE	6.6	2.4	2.13	552	
DBT-BZ-PXZ	AIE+TADF	26.6	27.9	9.2	557	Chem. Mater. 2017, 29, 3623[S2]
DBT-BZ-PTZ	AIE+TADF	26.5	29.1	9.7	563	
SBDBQ-DMAC	AIE+TADF	35.4	32.7	10.1	544	Chem. Sci. 2018, 9, 1385[S3]
DBQ-3DMAC	AIE+TADF	41.2	45.4	12.0	548	
PTZ-XT	AIE+TADF	16.7	7.6	11.0	553	Polym. J. 2017, 49, 197[S4]
CP-BP-PXZ	AIE+TADF	59.1	65.7	18.4	548	Angew. Chem. Int. Ed. 2017, 129, 13151[S5]
CP-BP-PTZ	AIE+TADF	46.1	55.7	15.3	554	
CCDD	AIE+TADF	39.8	41.7	12.7	543	Mater. Chem. Front. 2017, 1, 2039[S6]

DBQPXZ	AIE+TADF	24.9	19.6	8.8	564	Chem. Commun. 2018, 54, 1379[S7]
SFDBQPXZ	AIE+TADF	24.3	22.5	10.1	584	
DFDBQPXZ	AIE+TADF	21.0	20.6	9.8	588	
PCZ-CB-TRZ	AIE+TADF	16.7	7.6	11.0	586	Angew. Chem. Int. Ed. 2016, 55, 7171[S8]
ND-AC	**AIE+TADF**	**38.5**	**30.2**	**12.0**	**558**	**This work**

[S1] L. Chen, Y. Jiang, H. Nie, P. Lu, H. H. Y. Sung, I. D. Williams, H. S. Kwok, F. Huang, A. Qin, Z. Zhao, B. Z. Tang, *Adv. Funct. Mater.*, 2014, **24**, 3621.

[S2] J. Guo, X.-L. Li, H. Nie, W. Luo, R. Hu, A. Qin, Z. Zhao, S.-J. Su, B. Z. Tang, *Chem. Mater.*, 2017, **29**, 3623.

[S3] L. Yu, Z. Wu, G. Xie, W. Zeng, D. Ma, C. Yang, *Chem. Sci.*, 2018, **9**, 1385-1391.

[S4] N. Aizawa, C.-J. Tsou, I. S. Park, T. Yasuda, *Polym. J.*, 2017, **49**, 197.

[S5] J. Huang, H. Nie, J. Zeng, Z. Zhuang, S. Gan, Y. Cai, J. Guo, S.-J. Su, Z. Zhao, B. Z. Tang, *Angew. Chem. Int. Ed.*, 2017, **129**, 13151.

[S6] H. Zhao, Z. Wang, X. Cai, K. Liu, Z. He, X. Liu, Y. Cao, S.-J. Su, *Mater. Chem. Front.*, 2017, **1**, 2039.

[S7] L. Yu, Z. Wu, G. Xie, C. Zhong, Z. Zhu, D. Ma, C. Yang, *Chem. Commun.*, 2018, **54**, 1379-1382.

[S8] R. Furue, T. Nishimoto, I. S. Park, J. Lee, T. Yasuda, *Angew. Chem. Int. Ed.*, 2016, **55**, 7171–7175.